J. Fluid Mech. (2011), *vol.* 688, *pp.* 169–194.
doi:10.1017/jfm.2011.371

Frequency spectra evolution of two-dimensional focusing wave groups in finite depth water

Zhigang Tian[1,2], Marc Perlin[2] and Wooyoung Choi[1,3]†

[1] Division of Ocean Systems Engineering, Korea Advanced Institute of Science and Technology (KAIST), Daejeon 305-701, Republic of Korea

[2] Naval Architecture & Marine Engineering, University of Michigan, Ann Arbor, MI 48109, USA

[3] Department of Mathematical Sciences, New Jersey Institute of Technology, Newark, NJ 07102, USA

(Received 16 August 2010; revised 4 July 2011; accepted 2 September 2011; first published online 24 October 2011)

An experimental and numerical study of the evolution of frequency spectra of dispersive focusing wave groups in a two-dimensional wave tank is presented. Investigations of both non-breaking and breaking wave groups are performed. It is found that dispersive focusing is far more than linear superposition, and that it undergoes strongly nonlinear processes. For non-breaking wave groups, as the wave groups propagate spatial evolution of wave frequency spectra, spectral bandwidth, surface elevation skewness, and kurtosis are examined. Nonlinear energy transfer between the above-peak ($f/f_p = 1.2$–1.5) and the higher-frequency ($f/f_p = 1.5$–2.5) regions, with f_p being the spectral peak frequency, is demonstrated by tracking the energy level of the components in the focusing and defocusing process. Also shown is the nonlinear energy transfer to the lower-frequency components that cannot be detected easily by direct comparisons of the far upstream and downstream measurements. Energy dissipation in the spectral peak region ($f/f_p = 0.9$–1.1) and the energy gain in the higher-frequency region ($f/f_p = 1.5$–2.5) are quantified, and exhibit a dependence on the Benjamin–Feir Index (BFI). In the presence of wave breaking, the spectral bandwidth reduces as much as 40 % immediately following breaking and eventually becomes much smaller than its initial level. Energy levels in different frequency regions are examined. It is found that, before wave breaking onset, a large amount of energy is transferred from the above-peak region ($f/f_p = 1.2$–1.5) to the higher frequencies ($f/f_p = 1.5$–2.5), where energy is dissipated during the breaking events. It is demonstrated that the energy gain in the lower-frequency region is at least partially due to nonlinear energy transfer prior to wave breaking and that wave breaking may not necessarily increase the energy in this region. Complementary numerical studies for breaking waves are conducted using an eddy viscosity model previously developed by the current authors. It is demonstrated that the predicted spectral change after breaking agrees well with the experimental measurements.

Key words: surface gravity waves, wave breaking

† Email address for correspondence: wychoi@njit.edu

1. Introduction

Breaking waves play an important role in upper ocean dynamics. Wave breaking limits wave height and dissipates wave energy. It also enhances gas and heat exchange between air and sea by entraining air into the water, injecting spray into the atmosphere, and generating near surface turbulence.

Our understanding of breaking waves has been advanced by numerous studies (e.g. Rapp & Melville 1990; Perlin, He & Bernal 1996; Melville, Veron & White 2002; Banner & Peirson 2007; Drazen, Melville & Lenain 2008; Tian, Perlin & Choi 2008, 2010). Lab experiments serve as the most reliable method in the study of breaking waves, as numerical simulations fail or cannot fully represent the physics subsequent to wave breaking, and field observations lack the control required for detailed studies. In lab experiments, breaking waves are generated often by focusing wave energy at a desired time and spatial location (e.g. Rapp & Melville 1990) and by Benjamin–Feir instability (e.g. Benjamin & Feir 1967; Tulin & Waseda 1999). In this study, we focus mainly on dispersive focusing wave groups in laboratory experiments.

The evolution of two-dimensional wave groups due to Benjamin–Feir instability has been studied in numerous experiments (e.g. Lake *et al.* 1977; Melville 1982; Tulin & Waseda 1999), which typically focused on the energy transfer among different frequency components. Lake *et al.* (1977) observed periodic modulation and demodulation in the evolution of the wave groups (wave steepness, $ka \sim 0.1$) and the spectral peak downshift in the absence of wave breaking. Melville (1982) investigated wave groups ($ka \sim 0.2$) that evolved to breaking. They found that the wave groups evolve only in a partial recurrence fashion, 'tending to lower frequency'. In addition, the evolution of the wave spectra does not limit itself to a few frequency components but tends to generate a growing, continuous one. Tulin & Waseda (1999) further studied breaking effects on the evolution of the wave groups due to Benjamin–Feir instability. It was observed that frequency downshift may not necessarily occur for wave groups that experience incomplete recurrence in the absence of wave breaking. The energy transfer from the higher to lower sidebands increased due to the presence of strong breaking, which typically downshifts the spectral energy.

Compared to the study of modulationally unstable wave group evolution, experimental studies of the spectral evolution of dispersive focusing wave groups, especially those that lead to wave breaking, have been rare. A related, significant study was performed by Baldock, Swan & Taylor (1996), who examined the nonlinearity of the wave kinematics, as well as the energy transfer to the higher and lower harmonics in the wave focusing process. Their study showed strong nonlinear wave–wave interactions occurred and thus the process is highly nonlinear close to the focusing point. The nonlinearity of the wave group is demonstrated to increase with wave amplitude and decrease with increased spectral bandwidth. This finding is consistent with the evolution of wave groups due to the Benjamin–Feir instability, which is often characterized by the so-called Benjamin–Feir Index (BFI, Janssen 2003). The BFI is defined as the ratio of wave steepness to spectral bandwidth, which measures the relative importance of nonlinearity compared to linear dispersion. Based on the wave spectra measured at stations along their wave tank, nonlinear energy transfer and reversibility were demonstrated. The study reported few details of the evolution of the wave spectra and the spatial variation of the energy level in different frequency ranges. More importantly, wave breaking effects on the spectral evolution of the dispersive focusing wave groups were not considered.

Energy dissipation due to wave breaking is also an important subject. Previous studies typically include quantification of the total energy dissipated and

parametrization of the energy dissipation rate (e.g. Duncan 1981, 1983; Rapp & Melville 1990; Melville 1994; Banner & Peirson 2007; Drazen *et al.* 2008; Tian *et al.* 2010). One may also be interested in how energy is dissipated across a wave spectrum, which is often obtained with surface elevation measurements and subsequent fast Fourier transform (FFT).

Rapp & Melville (1990) examined the spatial evolution of wave frequency spectra of breaking wave groups and observed that most of the energy dissipated is from the high-frequency end of the first harmonic band (i.e. $f/f_p = 1.0$–2.0). Kway, Loh & Chan (1998) made similar observations for breaking wave groups of three types of wave spectra (i.e. constant-amplitude, constant-steepness, and Pierson–Moskowitz). Neither study attempted to quantify the spectral change due to wave breaking or the viscous related dissipation, which was shown to be significant in the determination of energy loss in breaking waves (Banner & Peirson 2007; Tian *et al.* 2010).

Meza, Zhang & Seymour (2000) estimated the free-wave energy dissipation in breaking waves, generated with dispersive focusing wave groups in a two-dimensional wave flume. Spectral distribution of free-wave energy dissipation was quantified. They found that almost all energy dissipation is from wave components higher than the peak frequency and a small portion ($\sim$10 %) of the energy lost from the higher-frequency wave components is gained by lower-frequency components. No significant change in the vicinity of the spectral peak after breaking was observed. Energy dissipation due to viscous effects was neglected in their study.

Recently, Yao & Wu (2004) reported an experimental study on energy dissipation of unsteady wave breaking in the presence of currents. Measurements of incipient breaking wave groups were made to estimate energy dissipation due to friction on the tank bottom and sidewalls. Findings on energy loss and gain across the wave spectra due to wave breaking were generally consistent with previous studies. For breakers on strong opposing currents, lower-frequency wave components were reported to gain up to 40 % of the energy lost by the higher-frequency wave components. Little energy change at the spectral peak was observed.

In this study, using the experimental data collected in Tian *et al.* (2010) to develop an eddy viscosity model for energy dissipation due to wave breaking, observations of the spatial evolution of wave frequency spectra of both non-breaking and breaking dispersive focusing wave groups are presented. In addition, detailed nonlinear energy transfer between different frequency ranges is monitored. The remainder of this paper is organized as follows. Section 2 describes our experimental set-up for both surface elevation measurement by wave probes and surface profile measurement with high-speed imaging. Section 3 presents our experimental results and observations on wave spectral evolution. Numerical simulations are provided in § 4. The last section presents our conclusions.

2. Experiments

Details of the experiments are presented in Tian *et al.* (2008, 2010). However, for the completeness of this study, a brief introduction of the breaking wave generation and the surface elevation measurement is provided as follows.

The experiments are conducted in a two-dimensional wave flume at the University of Michigan. The wave flume is 35 m long, 0.70 m wide, and filled with tap water to a depth of 0.62 m. A servo-controlled wedge-type wavemaker with auxiliary electronics is located at one end of the flume to generate wave trains; two stacks of 'horsehair' mats are placed at the opposite end to help damp incident waves.

Dispersive focusing wave groups are generated with a technique similar to that in Perlin *et al.* (1996). The resulting wave groups have approximately constant steepness wave spectra. By adjusting the gain (i.e. relative voltage) of the input signal to the wavemaker, both non-breaking and breaking waves can be generated. Most of our wave groups that lead to breaking have a single plunger, though very limited spilling occurs either upstream, or of less importance downstream in some cases. Table 1 presents some key parameters of the generated wave groups. As listed in the table, wave groups are categorized into five wave packets (i.e. W1, W2, W3, W4 and W5) based on wave group structure and centre wave frequencies specified in the input signal to the wavemaker; gain values (e.g. G1 and G2) are used to distinguish a wave group from others in each of the five wave packets. In this way, each wave group is designated uniquely (e.g. W1G3 and W2G4). Note that gain (e.g. G1) in one wave packet is not necessarily the same as that in another wave packet.

Temporal variation of surface elevations at desired locations along the wave flume is recorded by capacitance wave probes, along with other assisting hardware. The sampling rate for the wave probes in these measurements is 100 Hz. Note that analogue filters (Krohn-Hite) set at a low-pass frequency of 25 Hz are used in the measurement. Relying on the high repeatability of the experiment (Tian *et al.* 2010), we achieved surface elevation measurements at 33 wave stations along the wave tank.

The measurements have been used to study wave breaking criteria and kinematics and dynamics of breaking waves by Tian *et al.* (2008, 2010). In this study, we use temporal surface elevation measurements to examine the wave frequency spectral evolution of the two-dimensional dispersive focusing wave groups.

3. Experimental results

3.1. *Definitions*

Surface elevations measured at wave stations along the wave tank and fast Fourier transform (FFT) analysis are used to obtain the wave energy density spectrum, $S(f)$. Sampling time is truncated to 40.95 s (i.e. $T = 40.95$ s), corresponding to 4096 points, and the mean of the measurements is subtracted before applying the FFT. The forward transformation used is

$$N(f) = \int_t^{t+T} \eta(t) \mathrm{e}^{-2\pi \mathrm{i} f t} \, \mathrm{d}t. \tag{3.1}$$

Here, $N(f)$ is the Fourier transform of the surface elevation $\eta(t)$. Then the wave frequency spectrum is computed as $S(f) = 2\,|N(f)|^2 / T$. Note that $S(f)$ is a single-sided wave spectrum. At each station, three repeated surface elevation measurements are obtained to find three wave frequency spectra, from which the amplitudes of the Fourier components of the same frequency are averaged to determine a mean frequency spectrum. Then, following Rapp & Melville (1990), the mean wave frequency spectrum is smoothed by averaging over five adjacent spectral components.

Once the wave frequency spectrum is obtained, the wave spectral bandwidth is determined as $\upsilon = \sqrt{(m_0 m_2)/m_1^2 - 1}$ (Longuet-Higgins 1983), where m_i is the ith spectral moment, given by

$$m_i = \int_{f_{min}}^{f_{max}} (2\pi f)^i \, S(f) \, \mathrm{d}f. \tag{3.2}$$

In this study, the lower and upper cutoff frequencies, f_{min} and f_{max}, are set to $0.5 f_p$ and $2.5 f_p$, respectively, where f_p is the frequency associated with the spectral maximum.

Wave packet	Wave group ID	f_c (Hz)	f_p (Hz)	$\Delta f/f_p$	S_G	BFI$_S$	C_{gs} (m s^{-1})	x_b (m)	t_b (s)	$\nu_{eddy} \times 10^3$ (m^2 s^{-1})
W1	W1G1	1.11	0.95	0.31	0.32	1.03	0.85	13.7	25.1	—
	W1G2				0.38	1.25	0.84	12.4	23.0	1.01
	W1G3				0.46	1.52	0.84	11.3	21.2	1.20
W2	W2G1	1.23	0.90	0.35	0.27	0.76	0.86	13.4	31.2	—
	W2G2				0.35	0.99	0.86	13.6	30.9	0.86
	W2G3				0.41	1.18	0.86	12.6	29.4	1.17
	W2G4				0.47	1.33	0.86	12.5	29.3	1.65
W3	W3G1	1.24	1.03	0.21	0.29	1.42	0.79	15.0	30.7	—
	W3G2				0.36	1.72	0.79	14.0	29.7	0.71
	W3G3				0.44	2.14	0.78	13.2	28.3	1.12
	W3G4				0.50	2.41	0.78	13.1	28.3	1.50
W4	W4G1	1.50	1.03	0.38	0.28	0.73	0.71	17.4	50.0	—
	W4G2				0.39	1.03	0.71	16.9	48.4	0.62
	W4G3				0.54	1.43	0.71	15.4	45.3	1.03
	W4G4				0.67	1.76	0.70	14.2	43.8	1.23
W5	W5G1	1.55	1.25	0.20	0.26	1.32	0.66	12.8	34.6	—
	W5G2				0.48	2.42	0.64	11.7	32.7	0.55

TABLE 1. Summary of primary wave parameters: f_c, centre wave frequency specified in the input signal to the wavemaker; f_p, peak wave frequency; Δf, frequency bandwidth based on half of the maximum energy associated frequencies; S_G, global wave steepness; BFI$_S$, Benjamin–Feir Index, defined as $S_G/(\Delta f/f_p)$; C_{gs}, characteristic group velocity; x_b, horizontal location of the focusing/breaking points relative to the mean position of the wavemaker; t_b, wave group focusing/breaking time relative to the initial motion of the wavemaker; ν_{eddy}, estimated eddy viscosity used in the numerical simulations. See Tian *et al.* (2010) for details on the determination of S_G, C_{gs} and ν_{eddy}.

The energy outside this frequency range is very small and can be neglected. The wave spectral bandwidth can also be defined by the frequencies associated with half of the maximum energy, $\Delta f/f_p$. For a wave group with surface elevation obeying a Gaussian distribution, $\Delta f/f_p = \upsilon\sqrt{2\ln(2)}$. However, this relationship is not expected to be appropriate for our wave groups since they are non-Gaussian. Hereafter, to distinguish the two different bandwidths defined above, υ and $\Delta f/f_p$ are termed the spectral bandwidth and the frequency bandwidth, respectively.

The skewness λ_3 and the kurtosis λ_4 of the surface elevation can be evaluated, respectively, by the following definitions:

$$\lambda_3 = \frac{\langle \eta^3 \rangle}{\sigma^3}, \quad \lambda_4 = \frac{\langle \eta^4 \rangle}{\sigma^4}. \tag{3.3}$$

Here, σ is the standard deviation of the surface elevation, $\sigma^2 = \langle \eta^2 \rangle$, and the $\langle\rangle$ brackets indicate an ensemble average, i.e.

$$\sigma^2 = \langle \eta^2 \rangle = [\eta^2]/N = \left(\sum_{i=1}^{N} \eta_i^2 \right) \Big/ N. \tag{3.4}$$

(In our time series, the means have been set to zero via subtraction of the DC component.) Here, N is the number of samples used in the computation and the []

brackets represent a summation. The skewness λ_3 and the kurtosis λ_4 can be rewritten as

$$\lambda_3 = N^{1/2}\frac{[\eta^3]}{[\eta^2]^{3/2}}, \quad \lambda_4 = N\frac{[\eta^4]}{[\eta^2]^2}. \tag{3.5}$$

In our experiments, only one wave group is generated in each test and the recorded signal includes regions without waves (before and after the wave group arrives), which are necessarily excluded in the determination of σ, λ_3, and λ_4. Therefore, the duration of the time series has to be chosen carefully. To this end, we find the amplitude envelope of a surface elevation measurement using the Hilbert transform and use only the part of the measurement whose envelope is greater than one-twentieth of the maximum envelope. Using a different threshold will affect the magnitude of the computed skewness and the kurtosis. For example, a threshold of one-fortieth instead of one-twentieth gives approximately a 20 % and a 35 % increase in the maximum skewness and kurtosis achieved in the non-breaking focusing process, respectively; on the other hand, a threshold of one-tenth will decrease the maximum skewness and kurtosis by approximately 18 % and 25 %, respectively, for the non-breaking groups. However, the evolution behaviour of the two parameters, i.e. the general increase–decrease trend, remains the same. We remark that this may not be a concern for field measurements of continuous wave groups.

3.2. *Evolution of the non-breaking wave groups*

In this study, our wave groups are generated with a dispersive focusing technique. However, it is found that the focusing process is far from simple linear superposition, as we have observed a number of nonlinear features typically examined in wave groups subject to modulational instability. The following sections present our main findings.

Figure 1 exhibits a typical set of wave spectra evolution for a non-breaking wave group (W1G1). Figure 1(*a*) shows clearly the spectral change near the peak region while figure 1(*b*) demonstrates the variation of the higher- and lower-frequency components. As the wave group focuses, nonlinearity is featured and the energy gain in the higher-frequency components ($f/f_p > 1.5$) is evident. This energy 'leakage' to the higher-frequency components has been observed in previous studies (e.g. Baldock *et al.* 1996). This spectral change is attributed mainly to nonlinear energy transfer.

In the downstream defocusing process, the energy gain in the higher-frequency components disappears, possibly due to viscous dissipation and, partly, nonlinear energy transfer back to the spectral peak (see subsequent quantification results and figure 7). Overall, the energy in the frequency range $f/f_p = 0.9$–1.5 decreases significantly. This energy dissipation is attributed mainly to the nonlinear energy transfer to other frequency ranges along with viscous damping and the movement and dissipation caused by the contact lines on the sidewalls (Jiang, Perlin & Schultz 2004).

We also observed some energy variation in the lowest-frequency wave components ($f/f_p < 0.5$); however, no definite conclusions on energy change in this frequency range can be made based on our measurements. We note that Rapp & Melville (1990) observed considerable energy gain in the low-frequency components as an incipient breaking wave group approaches the focal point, and described it as 'growth of the forced wave at the low frequencies'.

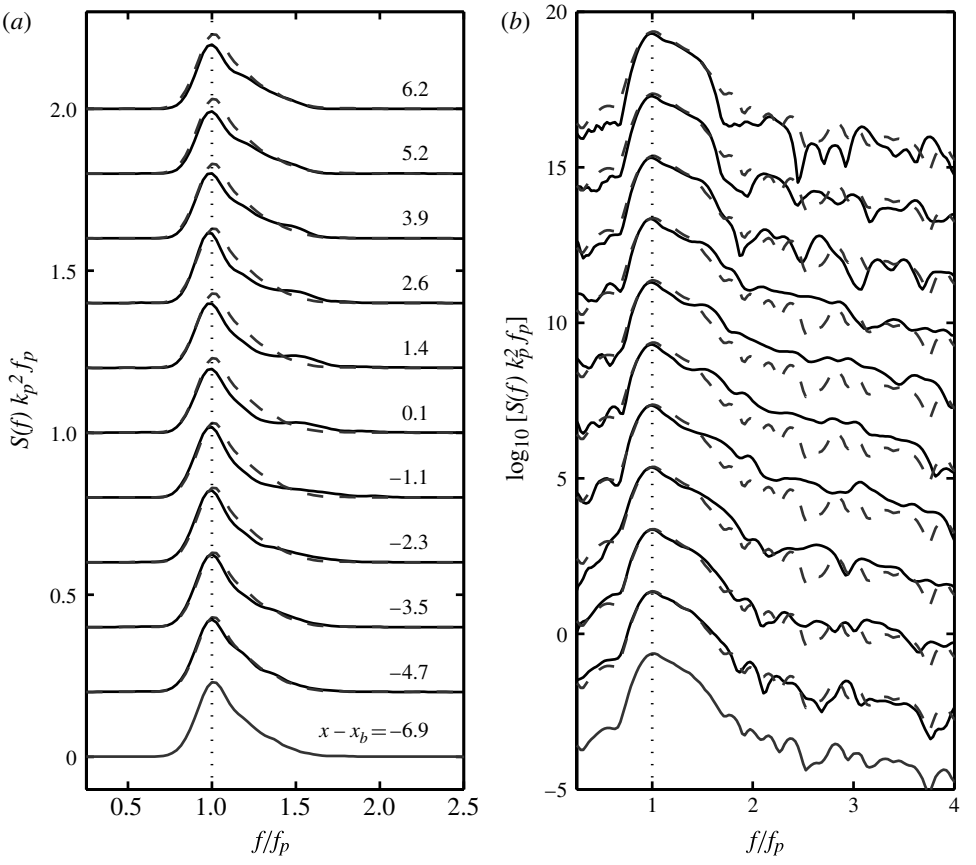

FIGURE 1. Evolution of the wave frequency spectra of a typical non-breaking wave group (W1G1): (*a*) linear scale and (*b*) logarithmic scale. Locations of measurements, $x - x_b$ (m), are shown in (*a*). The dashed lines indicate the reference spectrum measured at the first wave station ($x - x_b = -6.9$ m for this case). For clarity, an increment of 0.2 in (*a*) and 2.0 in (*b*) is applied along the ordinates to separate the wave spectra at different locations. The vertical dotted lines identify the initial peak frequency (i.e. $f/f_p = 1.0$).

3.2.1. *The spectral bandwidth, skewness and kurtosis*

By quantifying the spectral bandwidth (i.e. υ), the skewness and the kurtosis at wave stations along the tank, we can examine the wave spectral shape change as wave groups propagate. Figure 2 presents our results. The spectral bandwidth of the non-breaking wave groups is greater than 0.15, and therefore the wave groups are not that narrow-banded. As wave groups approach focusing, the spectral bandwidth increases 30–40 %, due mainly to the growth of the higher-frequency components. Therefore, the focusing process corresponds to wave spectral widening (i.e. energy transfer from the peak region to other frequency components due to both non-resonant and resonant nonlinear interaction). This energy redistribution suggests that the focusing process is far from linear superposition. In the defocusing process, the spectral bandwidth decreases, corresponding to a disappearance of the increased energy in the higher-frequency components. Interestingly, the spectral bandwidth recovers virtually to its initial level despite the evident spectral peak reduction, possibly due

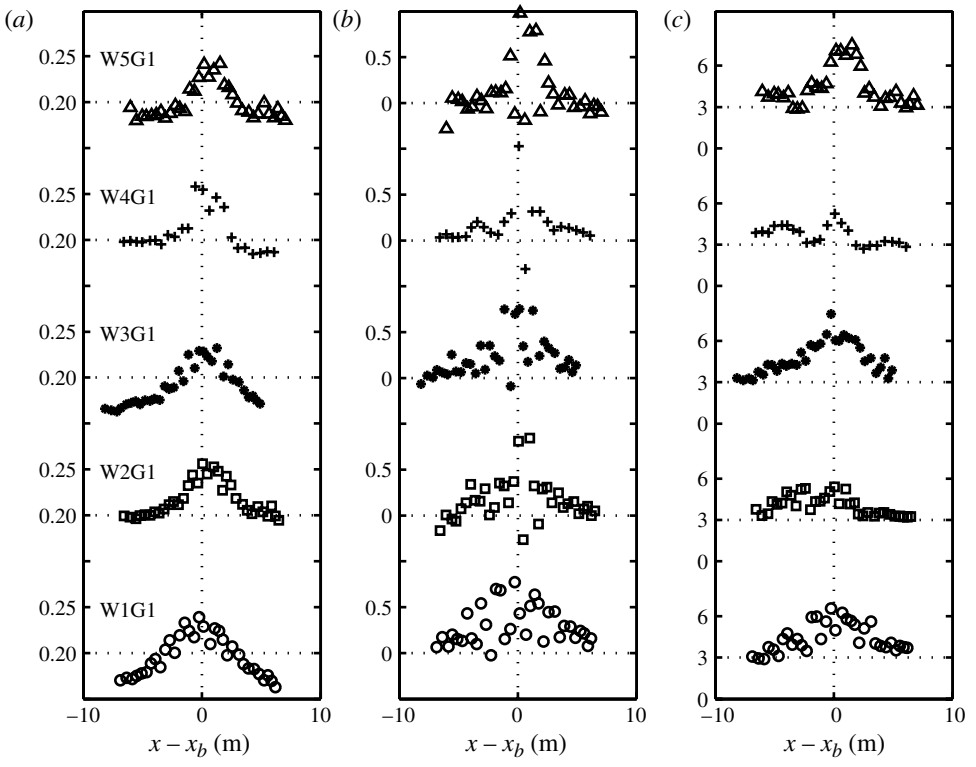

FIGURE 2. Spatial variation of (*a*) the spectral bandwidth, (*b*) surface-elevation skewness and (*c*) kurtosis for the non-breaking wave groups. Open circles represent W1G1; squares for W2G1; asterisks for W3G1; pluses for W4G1; triangles for W5G1. The abscissa represents the distance relative to the location of the wave focusing point, x_b: (*a*) υ; (*b*) λ_3; (*c*) λ_4.

to viscous related dissipation. The upstream and downstream spectral bandwidths are also approximately symmetric about the maxima for non-breaking conditions. On the other hand, the spectral bandwidth recovery is not observed in a recent laboratory study of unidirectional narrow-banded random waves (non-breaking) in deep water (Shemer & Sergeeva 2009). This discrepancy may be due to the fact that Shemer & Sergeeva (2009) investigated multiple wave groups that evolve in initially narrow-banded wavefields ($\upsilon < 0.12$), in which deterministic Gaussian-shaped unidirectional wave groups may interact continuously. On the other hand, we study the evolution of single dispersive focusing wave groups that have relatively broad-banded spectra ($\upsilon > 0.15$).

As for the skewness of the surface elevation in figure 2(*b*), the focusing–defocusing process corresponds in general to the growth reduction of the parameter. The general evolution behaviour of the skewness is expected as the parameter indicates the vertical (crest–trough) asymmetry of the surface elevation. Interestingly, in contrast to the general increasing trend as the wave groups focus, negative values of the skewness are observed close to the focusing points. This is due to the presence of deep troughs before and after the formation of sharp, high wave crests due to focusing. Similarly, the kurtosis of the surface elevation measures the peakedness of its probability distribution and its increase indicates typically the formation of extreme waves (Onorato *et al.* 2009). Therefore, as shown in figure 2(*c*), we observed

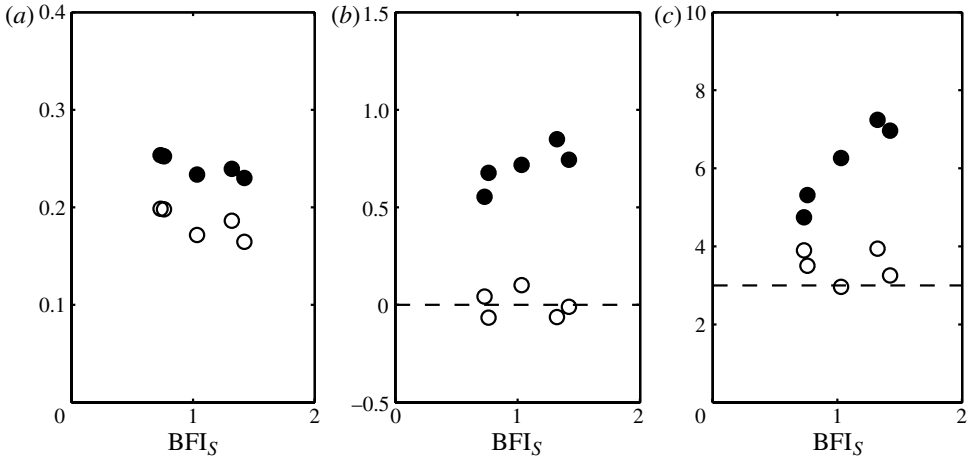

FIGURE 3. The maximum spectral bandwidth (a), skewness (b) and kurtosis (c) versus the BFI$_S$ for the non-breaking wave groups. Solid symbols, maximum value (averaged over the three greatest values) achieved in the wave focusing process; open symbols, initial value (averaged over the measurements at the first three probes): (a) υ; (b) λ_3; (c) λ_4.

an increase in the kurtosis in the generation of very steep waves due to dispersive focusing. Further downstream, both the skewness and the kurtosis nearly recover their initial levels. Notice that the magnitudes of the skewness and the kurtosis near the focusing points are much greater than those reported in previous studies (e.g. Shemer & Sergeeva 2009; Onorato *et al.* 2009), in which relatively long duration measurements of random wave fields are investigated. The discrepancy may be related to the surface elevation in our experiments in which only one dispersive focusing wave group is generated in each test.

It is our interest to examine the dependence of the spectral bandwidth, the skewness and the kurtosis on the so-called Benjamin–Feir Index (BFI; Janssen 2003), which is often employed to characterize wave evolution due to Benjamin–Feir instability. The BFI was defined originally as $\sqrt{2}\varepsilon/\sigma'$, where ε is a wave steepness based on wave spectral character and σ' is a relative frequency bandwidth. In this study, we use a similar parameter, $\mathrm{BFI}_S = S_G/(\Delta f/f_p)$. Here, S_G is a global wave steepness, $S_G = k_s \sum a_n$ (the same as the global wave steepness, S, in Tian *et al.* 2010); k_s is a characteristic wavenumber of the wave group as defined in Tian *et al.* (2010); a_n is the amplitude of the nth wave component. Both S_G and $\Delta f/f_p$ are determined and shown in table 1. The dependence of the maximum spectral bandwidth (i.e. υ), the skewness and the kurtosis presented as a function of the BFI$_S$ are shown in figure 3. Compared to their initial levels, the maximum spectral bandwidth shows no apparent dependence on the BFI$_S$ (i.e. the ratio of the maximum to the initial level remains approximately a constant). On the other hand, the maximum skewness and the kurtosis increase as the BFI$_S$ increases. This correlation suggests that the formation of very steep waves due to dispersive focusing (indicated by the kurtosis) in our non-breaking wave groups is more than just linear superposition; it involves nonlinear wave interactions in which the nonlinearity is represented by the BFI.

3.2.2. *Spectral distribution of the overall energy dissipation due to viscous related effects*

It is of interest to estimate the spectral distribution of the overall non-breaking energy dissipation. In the estimate, surface elevations measured at the first three

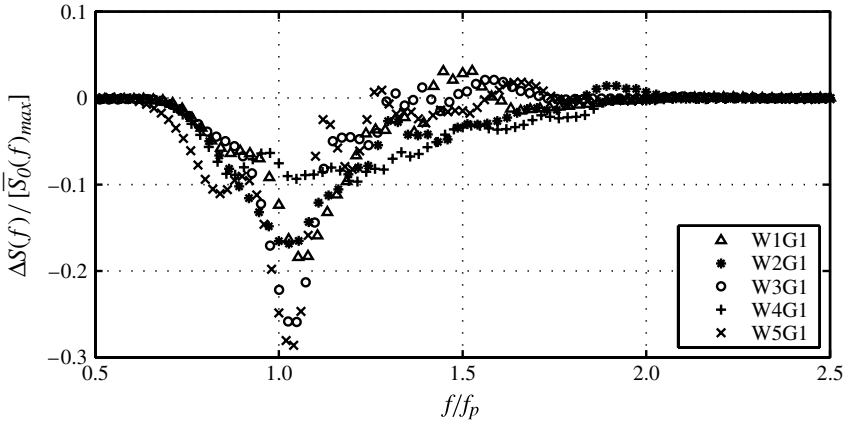

FIGURE 4. Spectral distribution of the non-breaking dissipation. $\overline{S_0}_{max}$ indicates the peak of the mean wave spectrum determined with the first three wave station measurements.

upstream and the last three downstream wave stations, far from the focusing points, are used. The mean spectral difference is found using

$$\begin{aligned}\Delta S(f) &= \overline{S_N}(f) - \overline{S_0}(f) \\ &= \frac{S_N(f) + S_{N-1}(f) + S_{N-2}(f) - S_1(f) - S_2(f) - S_3(f)}{3}.\end{aligned} \tag{3.6}$$

Here, $\overline{S_N}(f)$ indicates the mean wave spectrum determined with the last three wave station measurements and $\overline{S_0}(f)$ the mean wave spectrum over the first three station measurements. $S_i(f)$ is the wave spectrum determined at the ith wave station. The estimated mean spectral difference is non-dimensionalized by the peak of $\overline{S_0}(f)$. As shown in figure 4, the energy of wave components just above the peak decreases significantly (to $\sim$25 %), indicating that non-breaking energy dissipation is not negligible. In addition, most non-breaking energy dissipation appears in the vicinity of the spectral peak ($f/f_p = 0.9$–1.1) for wave groups with narrower frequency bandwidth (e.g. W3G1 and W5G1); on the other hand, for wave groups W2G1 and W4G1, non-breaking energy dissipation distribution is more uniform across the frequency spectrum, ranging from $0.75f_p$ to $2.0f_p$. This may be related to a frequency bandwidth effect.

Also obvious in figure 4, wave components in the lower-frequency region, $f/f_p = 0.5$–0.9, lose energy due to viscous related dissipation. Note that this result is based on direct comparison of the far upstream and downstream measurements only.

3.2.3. *Spatial evolution of the energy level in different frequency regions*

We now quantify the energy variation as a function of space by integrating the wave frequency spectrum obtained at each wave station. In the integration, only wave components with frequencies lower than $4f_p$ are included, as the higher-frequency components carry negligible energy (see figure 1). This energy as a function of space, $E_0(x)$, is shown in figure 5. In addition, we choose to examine the spatial variation of the energy in the spectral peak region ($f/f_p = 0.9$–1.1), $E_1(x)$. In the figure, we can see that the total non-breaking dissipation, ΔE_0 (energy difference between the mean of the first three and that of the last three measurements for each wave group shown in figure 5), is approximately 20 % of the initial energy after a distance of roughly 13 m

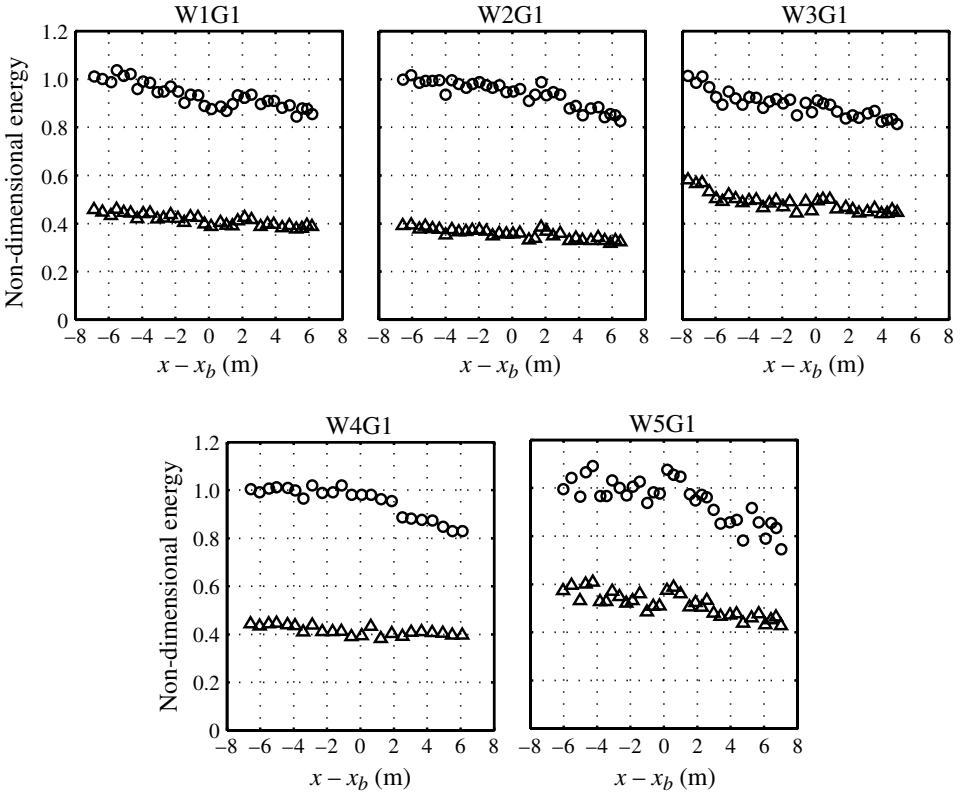

FIGURE 5. Energy levels as a function of space for the non-breaking wave groups. Circles, $E_0(x)/E_{0M}$; triangles, $E_1(x)/E_{0M}$. Here, $E_0(x)$ and $E_1(x)$ are the total energy ($f/f_p < 4$) and the energy near the spectral peak ($f/f_p = 0.9$–1.1), respectively; E_{0M} is the mean of the total energy measured at the first three wave stations. The abscissa indicates the distance relative to the wave focusing point, i.e. $x - x_b$ (m). Here, x_b is the horizontal location of the wave focusing point.

or approximately 10 wave lengths (i.e. $20\pi/k_p$). One comment is appropriate on the magnitude of the total non-breaking energy dissipation: viscous dissipation (including viscous dissipation on the water surface and frictional loss on the sidewalls and tank bottom) based on linear theory, i.e. exponential decay prediction (e.g. Mei 1983), accounts for only half of the total non-breaking dissipation observed (Rapp & Melville 1990; Tian *et al.* 2010). This suggests that the highly dissipative contact lines and capillary waves generated by water–sidewall interaction (Perlin & Schultz 2000; Jiang *et al.* 2004) also account for approximately half of the total non-breaking dissipation.

The total spectral peak dissipation, ΔE_1 (defined similarly to ΔE_0 but for energy in the spectral peak region), may be due to nonlinear energy transfer to other frequency ranges and viscous related effects. We observed that the dissipation contributes about 25–80 % of the total non-breaking energy dissipation. This contribution appears to depend on the BFI_S, i.e. the frequency bandwidth, $\Delta f/f_p$, and the wave steepness, S_G, of the wave groups. Figure 6 demonstrates the correlation between BFI_S and the spectral peak dissipation. An approximate linear correlation is apparent. This relationship indicates that the relative spectral peak dissipation, $\Delta E_1/\Delta E_0$, may be a nonlinear process. This observation may be the result of nonlinear energy transfer to

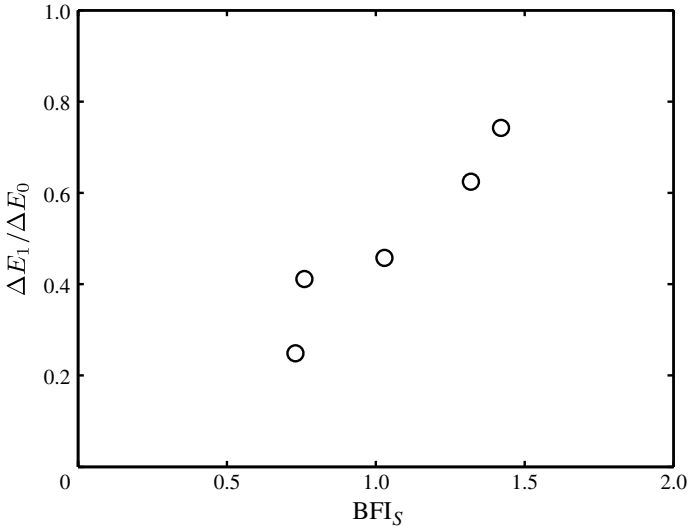

FIGURE 6. Correlation between the normalized spectral peak dissipation and our modified Benjamin–Feir Index. ΔE_1 and ΔE_0 are the total spectral peak dissipation and the total non-breaking dissipation, respectively.

higher-frequency components and/or nonlinear dissipation at the sidewalls. To the best of our knowledge, similar observations on the frequency bandwidth and the nonlinear effect on the spectral peak dissipation have not been reported previously.

We also choose to examine the spatial variation of the energy in two frequency regions, $E_2(x)$ for the above-peak range ($f/f_p = 1.2$–1.5) and $E_3(x)$ for the higher-frequency range ($f/f_p = 1.5$–2.5), and present the results in figure 7 for the non-breaking wave groups. (Note that the examination of the energy change in a lower-frequency region, $f/f_p = 0.5$–0.9, is also considered, and is presented subsequently in figure 14.) As the non-breaking wave groups focus, energy increase in the higher-frequency components is accompanied by energy decrease of the above-peak frequency components. In the defocusing process, the reverse occurs. The results suggest the presence and the reversibility of the nonlinear energy transfer between the above-peak and the higher-frequency components in the evolution of dispersive focusing wave groups. The energy transfer trend appears to be qualitatively similar to the spectral evolution due to Benjamin–Feir instability (e.g. Tulin & Waseda 1999). This nonlinear energy transfer should be related not only to the nonlinearity of the wave groups, but also to the frequency bandwidth, i.e. this transfer may be related to the BFI. In fact, the energy transfer is more evident for wave groups W1G1, W3G1 and W5G1, whose Benjamin–Feir Indices are among the largest of the five non-breaking wave groups. Similar to the spectral peak dissipation, the energy gain in the higher-frequency components demonstrates an approximately linear correlation with the BFI_S, as shown in figure 8 (although the data are limited).

3.3. *Evolution of the breaking wave groups*

Figure 9 presents typical wave frequency spectral evolution for two breaking wave groups, W1G2 and W1G3. As the wave groups focus, the tails of the wave spectra rise rapidly just prior to breaking, as can be seen from those results, for example, at $x - x_b = -0.5$ and -0.7 for W1G2 and W1G3, respectively. However, the spectra

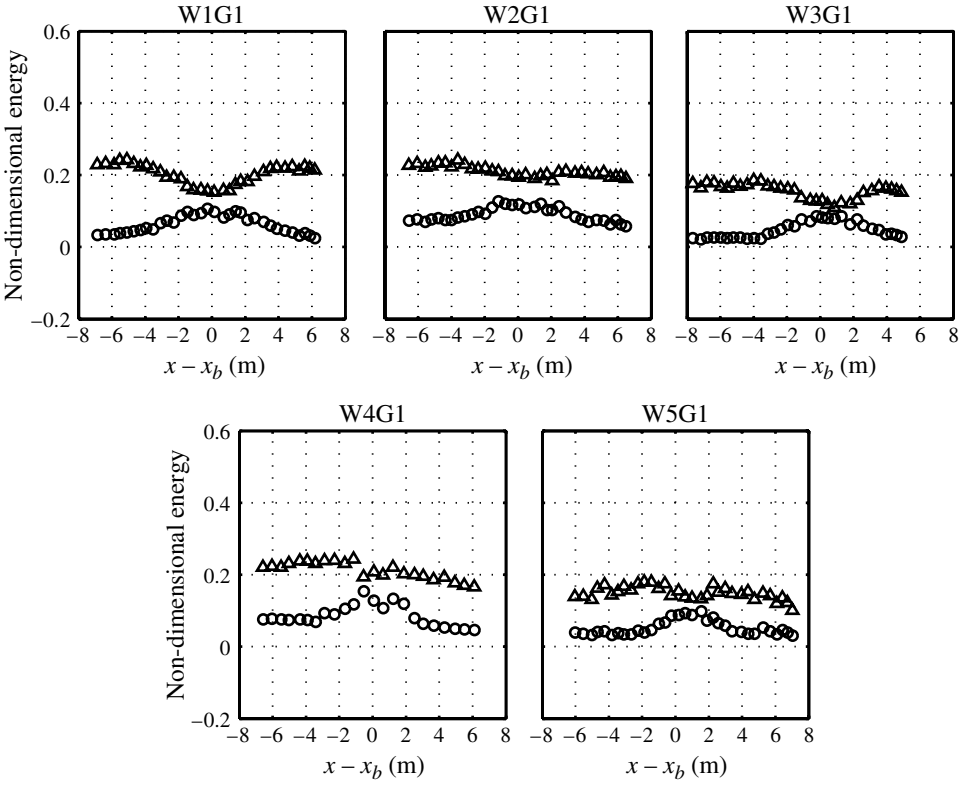

FIGURE 7. Nonlinear energy transfer between the above-peak and the higher-frequency components for the non-breaking wave groups. Triangles, $E_2(x)/E_{0M}$; circles, $E_3(x)/E_{0M}$. Here, $E_2(x)$ and $E_3(x)$ are energy in the above-peak ($f/f_p = 1.2$–1.5) and the higher-frequency regions ($f/f_p = 1.5$–2.5), respectively; E_{0M} is the mean of the total energy measured at the first three wave stations.

return almost to their initial energy levels following wave breaking. In general, the wave components of frequencies higher than the spectral peak appear to lose energy, as a result of both non-breaking loss (i.e. viscous related effects) and wave breaking. As wave breaking intensifies (e.g. W1G3 versus W1G2), more energy loss is observed. While the energy loss near the spectral peak may be mainly due to nonlinear energy transfer and viscous related effects, the energy loss in the frequency range of $f/f_p = 1.2$–2.0 may be attributed primarily to wave breaking. Rapp & Melville (1990), for example, observed that most of the total energy loss was in the higher-frequency end of the first harmonic band (i.e. $f/f_p = 1.0$–2.0) and the second harmonic band (i.e. $f/f_p = 2.0$–3.0). Also apparent in figure 9 is the slight downshift of the spectral peak frequency, which is possibly due to the presence of strong nonlinearity and wave breaking. This is evident from the peak deviation from the initial frequency peak shown by the vertical dotted lines in the figure.

3.3.1. *Evolution of the spectral bandwidth, skewness and kurtosis*

We examined the evolution of the spectral bandwidth of the breaking wave groups and present the results in figure 10. As shown, the spectral bandwidth achieved its maximum immediately before wave breaking and, compared to the non-breaking wave groups, the maximum spectral bandwidth is much larger. The increase of the spectral

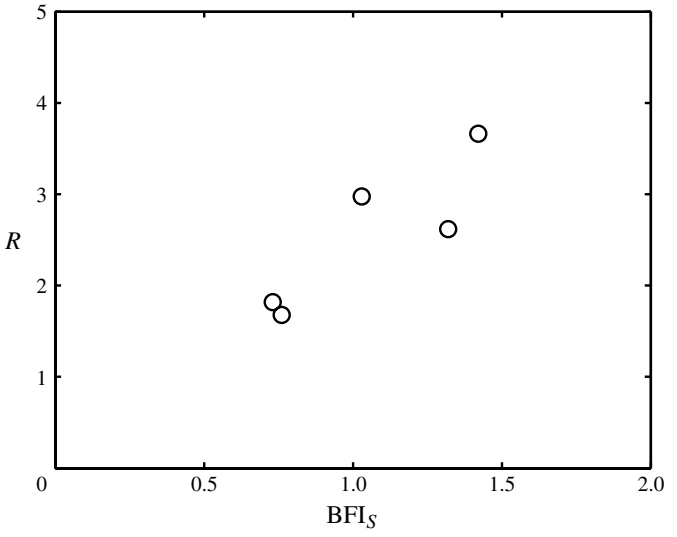

FIGURE 8. Correlation between the energy gain in the higher-frequency range and the BFI$_S$. $R = E_{3max}/E_{30}$. Here, E_{30} is the initial energy in the higher-frequency region ($f/f_p = 1.5$–2.5), an average of the measurements at the first three wave stations; E_{3max} is the maximum energy in the frequency range due to energy transfer (averaged over the three largest values).

bandwidth suggests the redistribution of the energy across the wave spectrum via nonlinear energy transfers. After breaking, the spectral bandwidth reduced as much as 40 % within one wave length ($2\pi/k_p$), mainly due to the energy loss in the above-peak and higher-frequency ranges during the breaking events. Compared to the virtually full recovery of the spectral bandwidth in the non-breaking wave groups, this spectral bandwidth does not recover to its initial level due to wave breaking.

As for the skewness and the kurtosis of the surface elevation in the breaking wave groups, their growth–decay evolution trends are qualitatively similar to, but not as clear as those of the non-breaking wave groups. The breaking wave groups in general have larger, positive skewnesses, indicating a greater crest–trough asymmetry. In addition, for some of the breaking wave groups, the kurtosis of the surface elevation remains at an approximately constant level even well after breaking, i.e. over a certain distance, although it returns to the original level for some wave groups (e.g. W2G4). This behaviour is different from the non-breaking wave groups and the reason for the difference is not yet understood.

The maximum spectral bandwidth, skewness and kurtosis presented in the breaking wave groups are shown in figure 11. Similar to the non-breaking wave groups, the ratio of the maximum to the initial spectral bandwidth in the breaking wave groups remains at an approximately constant level. As for the maximum skewness and kurtosis presented for the breaking groups, no apparent dependence on the BFI$_S$ is observed, which is inconsistent with that of the non-breaking wave groups. This discrepancy may be due to the presence of wave breaking.

In this study, surface elevation measured at the first wave station is used to determine the initial Benjamin–Feir Index; however, alternatively, measurements at downstream wave stations could be used to compute local BFIs that may change rapidly in the evolution of the wave groups (Janssen 2003). When local BFIs are determined at the wave stations where the maximum skewness and kurtosis are

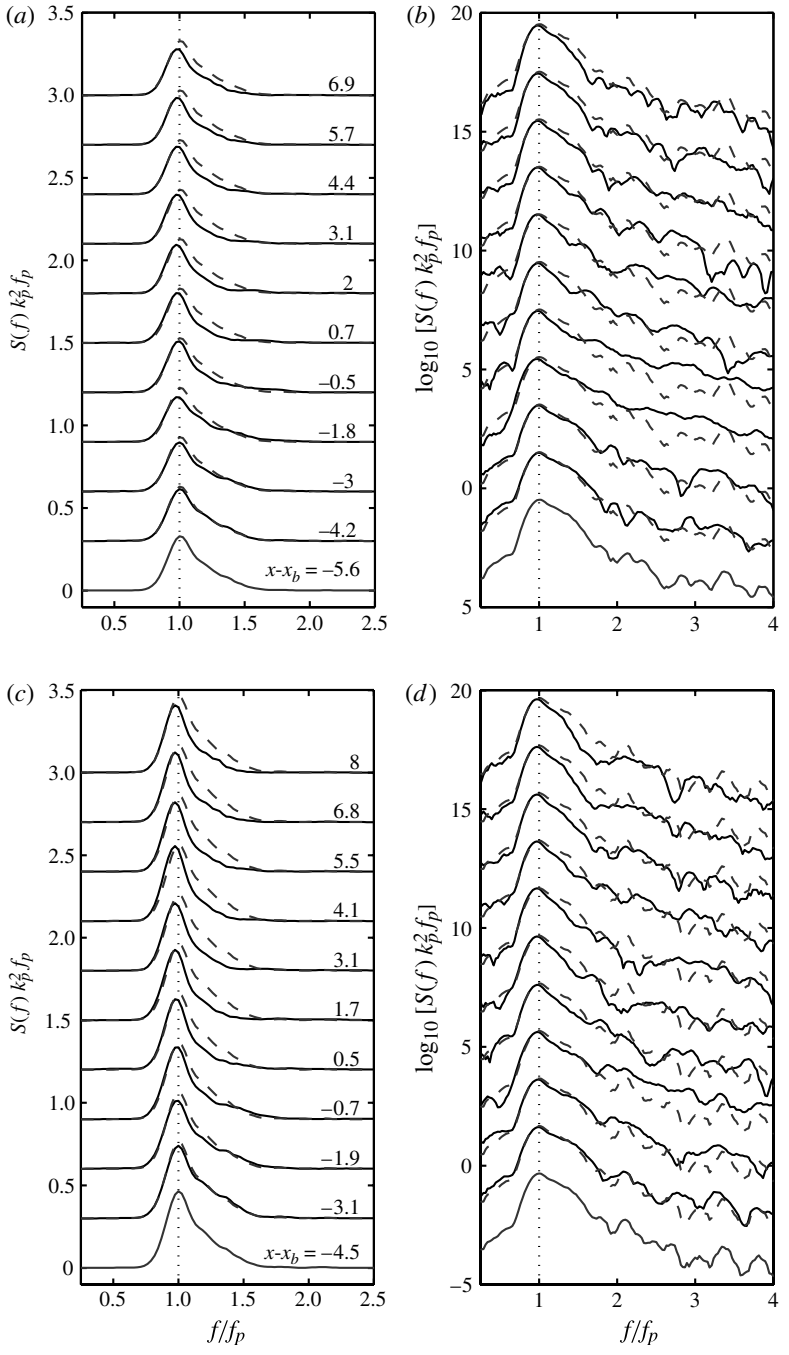

FIGURE 9. Evolution of the wave frequency spectra for two typical breaking wave groups: (*a*,*b*) W1G2 and (*c*,*d*) W1G3. Locations of measurements, $x - x_b$ (m), are shown in the linear scale graphs (*a*,*c*). The dashed lines indicate the reference spectrum measured at the first wave station. For clarity, an increment of 0.2 in the linear scale graphs (*a*,*c*) and 2.0 in the logarithmic scale graphs (*b*,*d*) are applied along the ordinates to separate the wave spectra at different locations. The vertical dotted lines identify the initial peak frequency (i.e. $f/f_p = 1.0$).

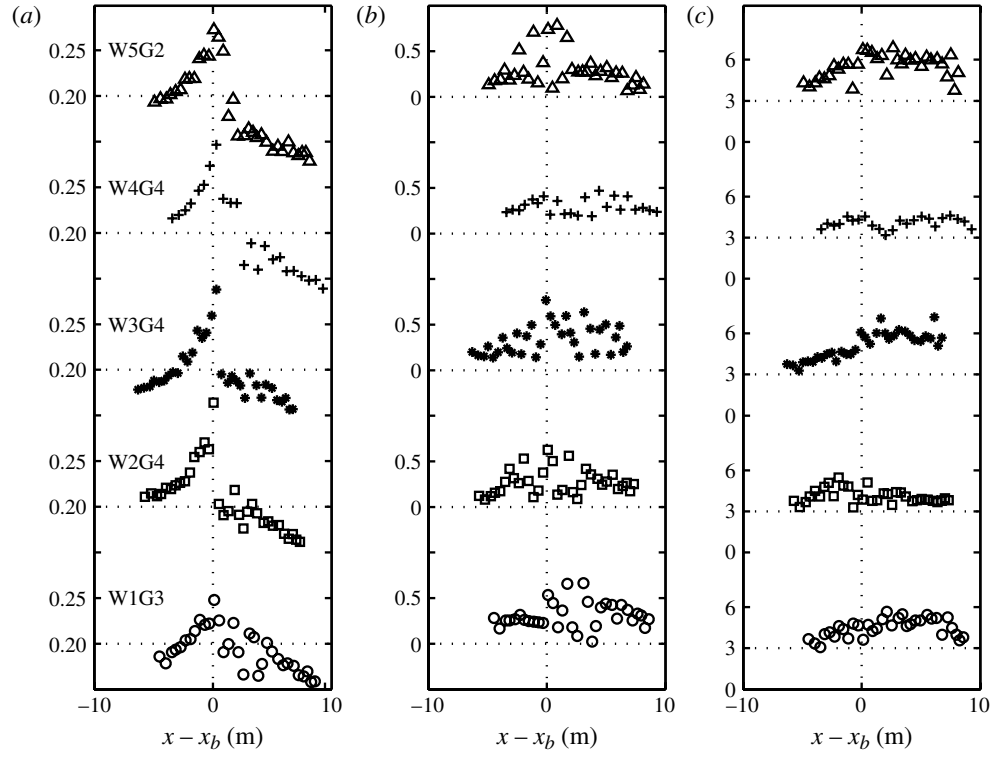

FIGURE 10. Spatial variation of (*a*) the spectral bandwidth, (*b*) surface elevation skewness and (*c*) kurtosis for the five violent breaking wave groups. Open circles represent W1G3; squares for W2G4; asterisks for W3G4; pluses for W4G4; triangles for W5G2: (*a*) υ; (*b*) λ_3; (*c*) λ_4.

achieved, we found that they are in general greater than the initial ones, but no definite correlations between the local BFIs and the maximum skewness and kurtosis can be identified for both the non-breaking and the breaking groups.

3.3.2. *Spectral distribution of the overall energy variation due to wave breaking and nonlinear energy transfer*

The overall spectral variation of breaking wave groups is due to three factors, i.e. wave breaking, nonlinear energy transfer among different frequency components and viscous related dissipation. In this section, we intend to determine the spectral variation mainly due to the first two factors, i.e. eliminating or minimizing that due to viscous related dissipation. For this purpose, two typical methods using surface elevations measured at stations before and after wave breaking are available. In one method, one may obtain this spectral variation by comparing wave frequency spectra immediately upstream and downstream of breaking. Non-breaking dissipation has a minimal effect over this short distance; this minimal change was ignored by Meza *et al.* (2000). According to Meza *et al.* (2000), wave spectra at locations near breaking vary considerably in lower and higher frequencies due to the generation of bound waves. Therefore, special treatment, i.e. bound wave removal, is necessary. Alternatively, Yao & Wu (2004) proposed using wave frequency spectra measured far from breaking, where they assumed few bound waves were present. In this method, the spectral variation due to non-breaking dissipation of a non-breaking wave group is

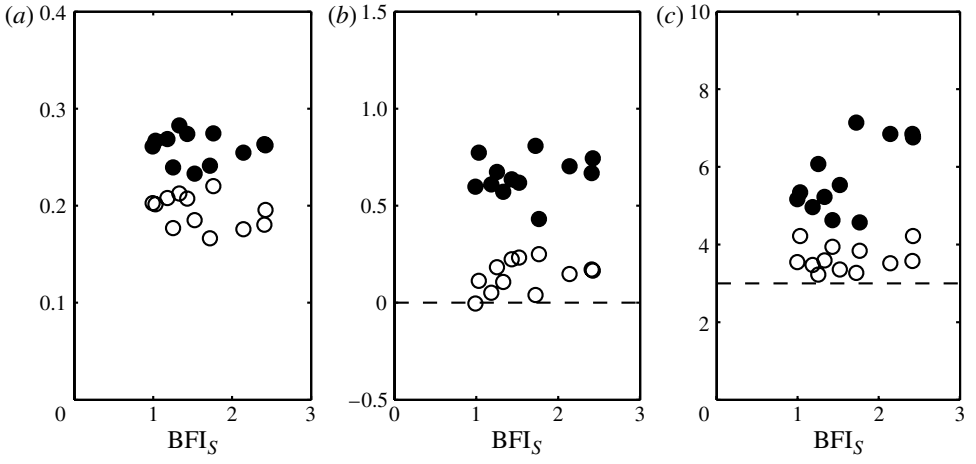

FIGURE 11. The maximum spectral bandwidth (a), skewness (b) and kurtosis (c) versus the BFI$_S$ for the breaking wave groups. Solid symbols, maximum value (averaged over the three greatest values) achieved in the wave focusing process; open symbols, initial value (averaged over the measurements at the first three probes): (a) υ; (b) λ_3; (c) λ_4.

estimated first. Then the spectral change of a breaking wave group, representing non-breaking dissipation, variation due to nonlinear energy transfer and breaking loss, is estimated accordingly. Finally, the spectral distribution of the overall energy variation due to wave breaking and nonlinear energy transfer can be determined by comparing the two estimates.

In this study, we employ the second technique to determine the spectral variation for the breaking waves. Equation (3.6) is used to estimate the spectral changes, $\overline{\Delta S_{tb}}(f)$ and $\overline{\Delta S_{nb}}(f)$, for the breaking waves and the corresponding non-breaking wave groups, respectively. Then the non-breaking dissipation is subtracted from the total spectral change for the breaking waves, i.e. $\overline{\Delta S_b}(f) = \overline{\Delta S_{tb}}(f) - \overline{\Delta S_{nb}}(f)$. We note that both $\overline{\Delta S_{tb}}(f)$ and $\overline{\Delta S_{nb}}(f)$ are non-dimensionalized with the peak of the corresponding upstream reference spectrum before the subtraction. In addition, for a fair estimation of the spectral change due to viscous related dissipation in the breaking wave groups, measurements at comparable distance relative to wave focusing/breaking points, i.e. $x - x_b = -5$ m for upstream and 5 m for downstream, are used. For the three cases in which the maximum relative distance upstream to x_b is less than 5 m (e.g. W4G4), the first probe measurements are used. With the advent of this method, we produced figure 12, which exhibits the spectral changes for the breaking wave groups. As we have removed, as far as possible, the spectral change due to viscous related dissipation, the spectral variation is caused primarily by wave breaking and nonlinear energy transfer. As discussed later (see § 3.3.3), the spectral change in the higher-frequency components, roughly from $f/f_p = 1.2$–2.0, is due primarily to wave breaking, and in general the total energy loss in the range increases as wave breaking intensifies.

Also in figure 12, the energy gain of the lower-frequency region, $f/f_p = 0.5$–0.9, may be related to energy redistribution (e.g. frequency downshift) due to nonlinear energy transfer. This energy gain appears to increase as the nonlinearity increases for wave groups with similar structure, as expected. Note that nonlinear energy transfer to the lower-frequency region in the focusing process is evident (as discussed in § 3.3.3

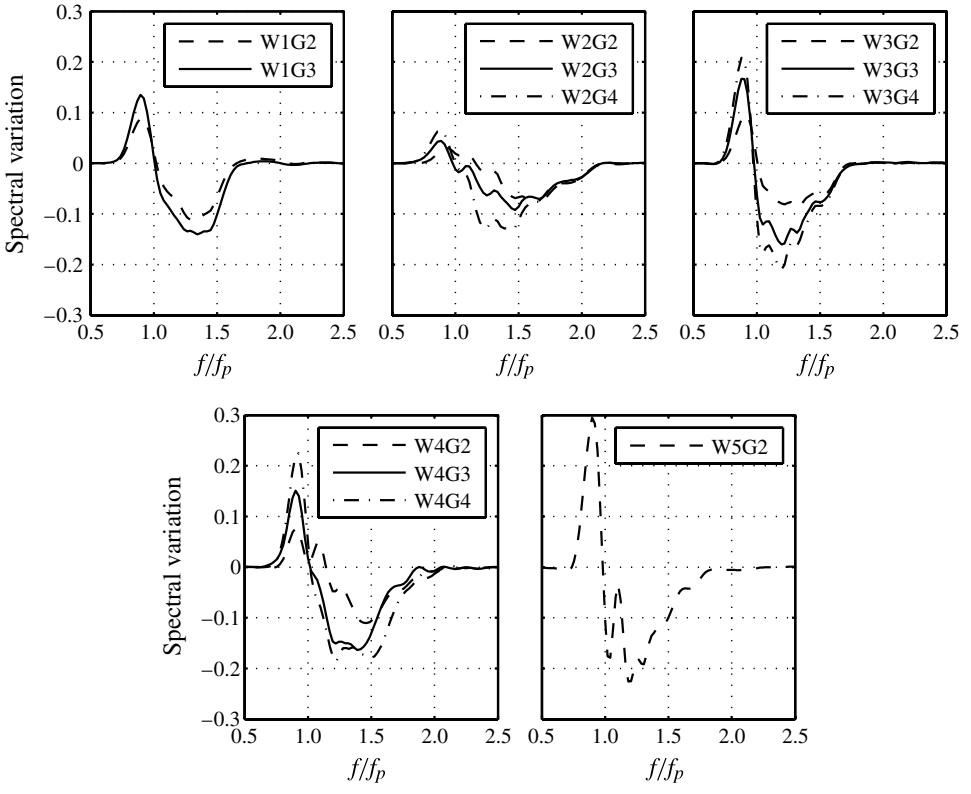

FIGURE 12. Wave frequency spectral variation, $\overline{\Delta S_b}(f)$, for the breaking wave groups. This spectral variation is due mainly to wave breaking and nonlinearity. The spectral change due to non-breaking dissipation is subtracted from the total spectral change of the breaking wave groups, i.e. $\overline{\Delta S_b}(f) = \overline{\Delta S_{tb}}(f) - \overline{\Delta S_{nb}}(f)$. Here, $\overline{\Delta S_{tb}}(f)$ is the total spectral change for the breaking waves and $\overline{\Delta S_{nb}}(f)$ are for the non-breaking ones. Both $\overline{\Delta S_{tb}}(f)$ and $\overline{\Delta S_{nb}}(f)$ are non-dimensionalized respectively with the peak of the reference spectrum at the first wave probe before the subtraction.

and shown in figure 14), and this energy transfer could be reversible in the absence of wave breaking, as discussed earlier.

3.3.3. *Spatial evolution of energy level in different frequency ranges for the breaking wave groups*

We present the total energy, as well as the energy in the spectral peak, the above-peak and the higher-frequency ranges, as a function of space for the breaking wave groups in figure 13. As shown in the figure, the total energy decreases gradually before wave breaking due to the viscous related effects (as much as 10 % after approximately three wave lengths); following breaking, the total energy continues to decay but at a much smaller rate (less than 5 % after 3 wave lengths), which may be attributed to the reduction in nonlinearity. Note that the total non-breaking dissipation for the non-breaking wave groups is approximately 20 % of the initial energy after a distance of roughly 10 wave lengths (i.e. $20\pi/k_p$). Depending on breaking strength, 10–25 % of the total energy is dissipated in a relatively short distance as a result of wave breaking.

As for the energy in the spectral peak region, both the energy and the spectral peak dissipation, i.e. $E_1(x)/E_{0M}$ and $\Delta E_1(x)/E_{0M}$, are comparable to the corresponding

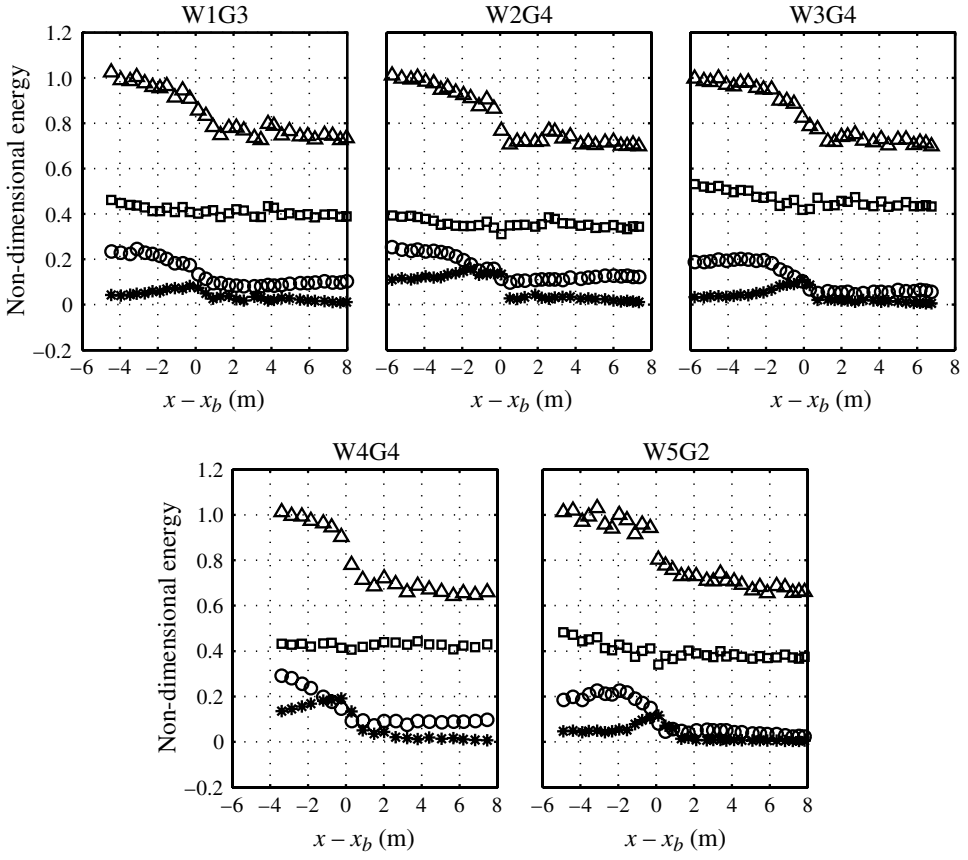

FIGURE 13. Energy levels as a function of space for the breaking wave groups (shown only for the most violent breaker among wave groups with similar structures). Triangles, $E_0(x)/E_{0M}$; squares, $E_1(x)/E_{0M}$; circles, $E_2(x)/E_{0M}$; asterisks, $E_3(x)/E_{0M}$. Here, $E_0(x)$ are the total energy ($f/f_p < 4$); $E_1(x)$ the energy near the spectral peak region; $E_2(x)$ the energy in the above-peak region; and $E_3(x)$ the energy in the higher-frequency region; E_{0M} is the mean of the total energy measured at the first three wave stations.

non-breaking wave groups (see figure 5 for a comparison with figure 13). In addition, the spectral peak energy dissipates gradually in general, even near wave breaking, which introduces rapid dissipation of $E_0(x)$. These observations suggest that the dissipation in the spectral peak region for the breaking waves is caused mainly by viscous related effects and nonlinear energy transfer to higher and lower frequency components. Therefore, it can be argued that wave breaking has no immediate impact on the spectral peak region. We note that the viscous related damping also dissipates energy in other frequency regions.

Also visible in figure 13, similar to the non-breaking wave groups, is the nonlinear energy transfer between the above-peak and the higher-frequency range before wave breaking occurs. As much as 10 % of the total initial energy, E_{0M}, is transferred from the above-peak frequency region (E_2) to the energy in the higher-frequency region (E_3). However, most of the energy gained in the higher-frequency range may not transfer back to the above-peak region after breaking as it is dissipated. The results show that energy transfers first to smaller-scale wave components (i.e. the higher frequencies)

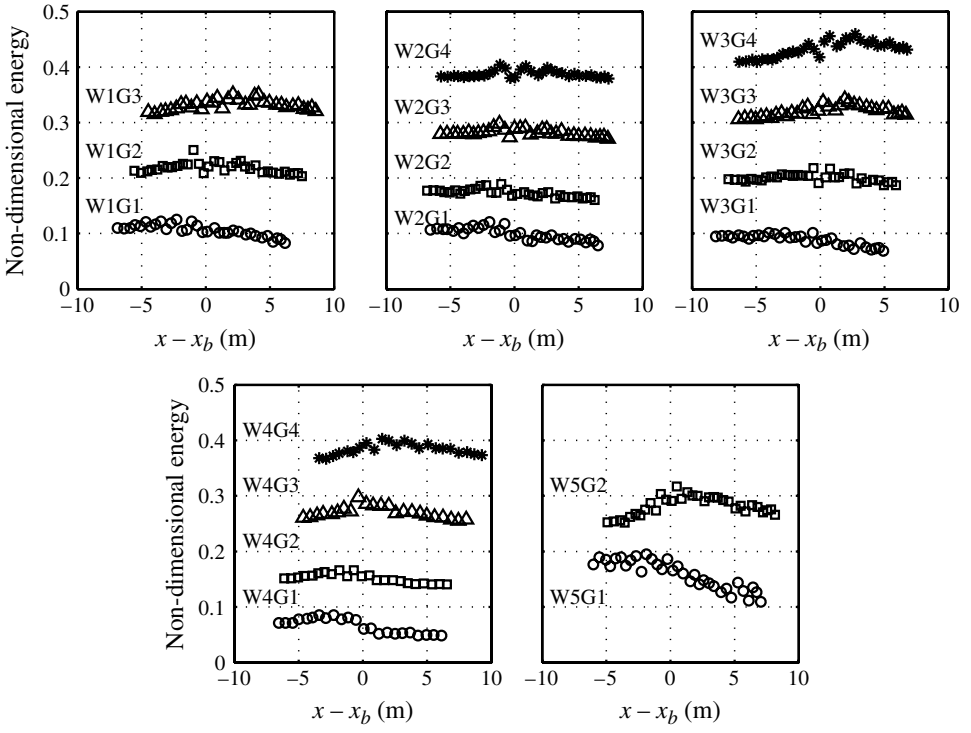

FIGURE 14. Energy in the lower-frequency region ($f/f_p = 0.5$–0.9) as a function of space, $E_4(x)/E_{0M}$. Here, E_{0M} is the mean of the total energy measured at the first three wave stations. Results for the non-breaking wave groups are represented by the open circles. For clarity, an increase of 0.1 is applied to the ordinate to distinguish wave groups with similar group structure but different gains.

and then dissipates in the breaking process. This may be similar to the so-called cascade decay of wave energy. However, we note that the energy transfer is due to nonlinearity rather than the outcome of wave breaking.

In addition, we examined the energy in even higher frequencies ($f/f_p = 2.5$–4) and found that the energy may increase or decrease, depending on specific wave groups, due to wave breaking. Therefore, wave breaking obviously dissipates energy, but whether the energy loss follows the so-called cascade decay is not clear. We note that a recent study (Gemmrich, Banner & Garrett 2008) showed that the wave energy loss is dominated by the intermediate scales, but not by the small-scale breakers in the field. Based on their field measurements, Gemmrich *et al.* (2008) argued that the cascade of wave energy decay may be unlikely.

Recent studies (e.g. Meza *et al.* 2000; Yao & Wu 2004) showed that wave breaking introduces energy gain in the lower-frequency wave components. To examine the spectral change in the lower-frequency region ($f/f_p = 0.5$–0.9), we determined energy in that region as a function of space, $E_4(x)$, and the results are provided in figure 14. For the non-breaking cases, it appears that the energy in this frequency region remains virtually at a constant level, despite some small variations, to the wave focusing point; on the other hand, the energy dissipates due to mainly viscous related effects in the defocusing process as wave groups evolve. This fact indicates that energy transfer to the lower-frequency region, possibly from the spectral peak and the above-peak ranges,

may have occurred in the focusing process so that it approximately compensates the dissipation due to viscous related effects.

For most of the breaking wave groups, we observed energy gain in the lower-frequency region prior to wave breaking, implying again the presence of nonlinear energy transfer (which is stronger compared with that in the non-breaking wave groups). In addition, in more than half of the 12 breakers, there is no obvious energy gain in the lower-frequency region immediately after breaking. These results indicate that the energy gain in the lower-frequency components (see figure 12) are possibly due to nonlinear energy transfer from other frequency ranges prior to wave breaking and that wave breaking may not necessarily increase the energy in this part of the spectrum, although it prevents the gained energy in the lower-frequency region from returning to other frequency regions. Previous studies have shown that the lower-frequency wave components gain energy due to wave breaking. We note that their conclusions are based on simple comparisons of measurements upstream and downstream of wave breaking rather than detailed examination of the spatial evolution of the energy in the lower-frequency components.

4. Numerical simulations

Tian *et al.* (2010) proposed an eddy viscosity model to simulate energy dissipation due to unsteady plunging breakers. In this study, complementary numerical simulations using this eddy viscosity model are conducted to examine its capability in predicting the spectral evolution of the wave groups. Details of the eddy viscosity model, the generation of the initial conditions, and the set-up for the numerical simulations are referred to Tian *et al.* (2010). The eddy viscosity used in the numerical simulations is of the order of 10^{-3} ($m^2\ s^{-1}$), as listed in table 1. Comparisons of the experimental and the numerical results follow.

Figure 15 provides comparisons between the experimental and numerical results of the surface elevation and the corresponding wave frequency spectra for three of the wave groups (i.e. W1G1, W1G2 and W1G3). As demonstrated in Tian *et al.* (2010) and shown in this figure, the eddy viscosity model predicts well the surface elevation for the wave groups, even in the presence of wave breaking. The agreement in the wave frequency spectrum is satisfactory, but is not as good as for the surface elevation. Since the energy spectrum is essentially wave amplitude squared as a function of frequency, the error in the surface elevation prediction is expected to be amplified in the wave spectrum prediction, consistent qualitatively with our observations. In a recent study by Shemer, Goulitski & Kit (2007, their figure 2), the surface elevation prediction for their non-breaking wave groups appears to be reasonable; on the other hand, their predicted frequency spectra also demonstrate larger discrepancies from their measurements.

In figure 15, the comparisons of the wave spectra at the upstream locations are accurate as these locations are close (within 2.5 m) to where the surface elevations are measured to initialize the numerical simulations. Close to the wave focusing/breaking points, both the experimental and the numerical results demonstrate the peak frequency downshift, which appears more obvious for increasingly nonlinear wave groups. The measurements and the predictions are qualitatively similar, but deviate somewhat. As wave groups propagate further downstream, the discrepancy becomes more apparent. The difference of the spectral peak magnitude between the measurement and the predictions is within 5–10 %. In addition, the magnitudes of the lower-frequency wave components are overestimated while the higher ones are underestimated in the

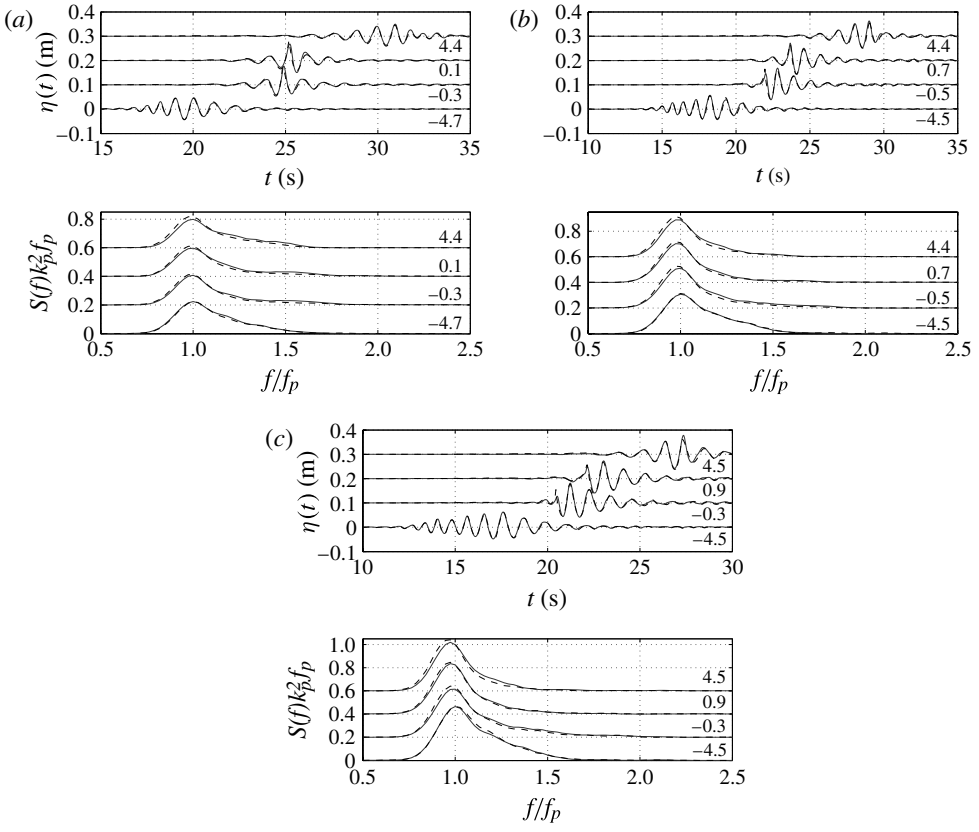

FIGURE 15. Comparisons between the experimental results of the surface elevation and the corresponding wave frequency spectra for a typical non-breaking wave group (W1G1) and two typical breaking wave groups (W1G2 and W1G3). Solid curves represent the experimental results and dashed curves are the numerical results. Locations relative to the wave focusing/breaking point, $x - x_b$ (m), are indicated to the right of each set of graphs. For clarity, increments of 0.1 and 0.2 are applied to the ordinates for the surface elevation and the wave spectra, respectively: (*a*) W1G1; (*b*) W1G2; (*c*) W1G3.

numerical predictions. One of the possible causes of the persistent difference for both non-breaking and breaking wave groups may be in applying to the free surface boundary conditions an effective viscosity that must account for the total non-breaking energy dissipation due to friction on the side tanks' walls and bottom as well as the contact line interactions in the experiments. Obviously this simple model with constant viscosity fails to describe accurately this frequency-dependent non-breaking energy dissipation. We note that the total energy of the predicted wave spectra is in general less than 5 % different from that of the experimental measurements. Nevertheless, further studies, e.g. comparison with experiments conducted in a wider tank where dissipation due to friction on the sidewalls is less important, are desirable.

Other than some disagreement in the comparisons of the measured and the predicted wave spectra, the simple eddy viscosity model appears to function generally well. As shown in figures 15(*b*) and 15(*c*), the relative change of the predicted wave spectra just after breaking (compared to the one close, but prior to wave breaking) is a good approximation to that of the measured spectra, suggesting that most of the

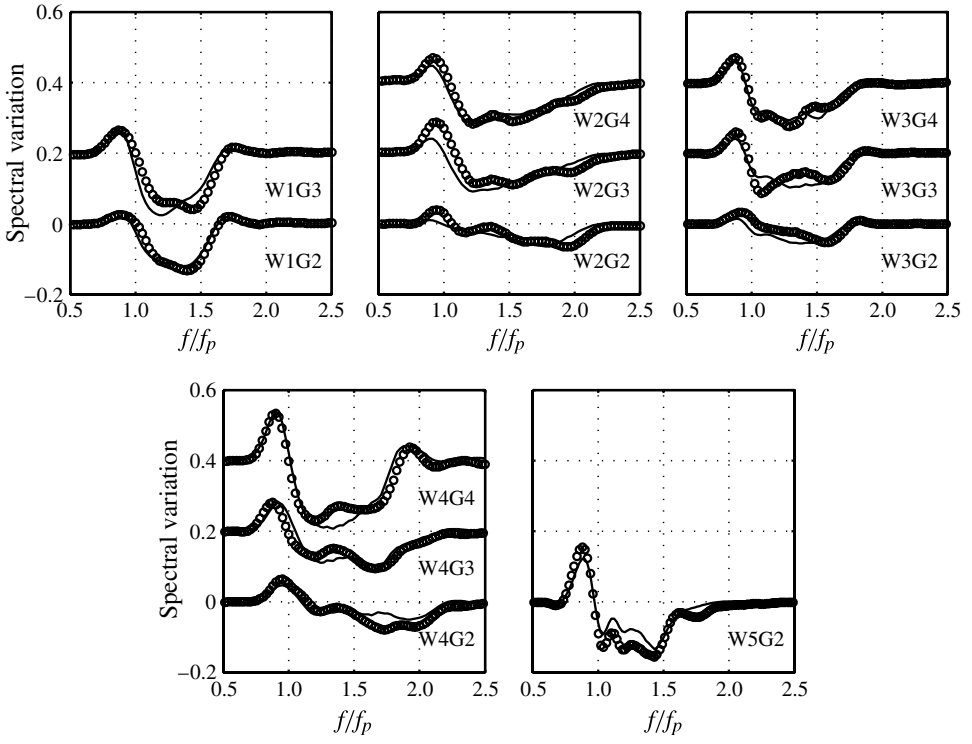

FIGURE 16. Comparison of the spectral variation based on numerical simulations (solid curves) and the measurements (open circles). The spectral variation is due primarily to wave breaking and nonlinearity. The procedure to determine the spectral change is similar to that used in constructing figure 12, but with measurements/numerical results close to the wave breaking points, i.e. $|x - x_b|2.5$ m. For clarity, an increment of 0.2 is applied to the ordinates in these graphs.

spectral variation due to wave breaking may have been captured by the eddy viscosity model. For further examination, we applied similar procedures used to determine the wave frequency variation for the breaking wave groups (figure 12) to the numerical predictions. Figure 16 provides a comparison of the spectral change, primarily due to wave breaking and nonlinearity, between the numerical and experimental results. In general, the spectral change immediately after wave breaking is simulated well by the eddy viscosity model. Considering the complicated kinematics and dynamics involved in breaking waves, the performance of this simple eddy viscosity model is much better than expected.

5. Conclusions

An experimental and numerical study of the evolution of two-dimensional dispersive focusing wave groups in finite depth water is presented. In the experiments, both non-breaking and breaking wave groups are generated via a dispersive focusing technique in a two-dimensional wave tank. Temporal variation of the surface elevation is measured with wave probes at fixed locations along the wave tank. Surface elevation measurements are used to examine the wave frequency spectral evolution, and to determine the spectral distribution of energy dissipation in both non-breaking and

breaking wave groups. It is found that the focusing process is far more complicated than simple linear superposition and nonlinear energy transfer between different frequency components is observed.

Spatial evolution of wave frequency spectra of the non-breaking wave groups is examined first. Wave spectral bandwidth and surface elevation skewness and kurtosis are inspected as the wave groups propagate. The spectral bandwidth increases due to nonlinear energy transfer across the frequency spectra during the focusing process, and reduces to its initial level far downstream. The vertical symmetry of the surface elevation (indicated by the skewness) and the formation of the very steep waves due to dispersive focusing (indicated by the kurtosis) show some correlation with the Benjamin–Feir Index (i.e. BFI_S). This suggests that the focusing process involves strong (both resonant and non-resonant) wave–wave interactions, whose nonlinearity may be characterized by BFI_S.

The nonlinear energy transfer between the above-peak and the higher-frequency regions and its reversibility in the non-breaking wave groups are demonstrated by the focusing and defocusing processes. Due to viscous effects and contact-line damping, about 20 % of the total energy is dissipated after a distance of 10 wave lengths in the non-breaking wave groups. Depending on the BFI_S, 25–80 % of this non-breaking energy loss is from the spectral peak region ($f/f_p = 0.9$–1.1). The non-dimensional energy loss in the spectral peak region rises as the BFI_S increases, suggesting this dissipation may be a nonlinear process. In addition, the energy gain in the higher-frequency region ($f/f_p = 1.5$–2.5) appears to have a strong dependence on the BFI_S. To the best of our knowledge, similar observations have not been reported previously. The spectral variation due to viscous related dissipation and nonlinear energy transfer is determined.

Observations of the evolution of the frequency spectra for the breaking wave groups are also reported. In the presence of wave breaking, the spectral bandwidth reduces significantly immediately after breaking and remains much smaller than its initial level. The dependence of the skewness and the kurtosis on the BFI_S becomes weak, compared to that of the non-breaking wave groups, due to the presence of wave breaking. Examination of the energy levels in different frequency regions is performed. It is found that the dissipation in the spectral peak region is due primarily to viscous related dissipation and nonlinear energy transfer. In addition, a significant amount of energy is transferred from the above-peak region ($f/f_p = 1.2$–1.5) to the higher frequencies ($f/f_p = 1.5$–2.5) before breaking. The energy in the higher-frequency region, as well as the energy transferred to the region, is dissipated during the breaking process. Nonlinear energy transfer also occurs from the spectral peak region to the lower-frequency region ($f/f_p = 0.5$–0.9) before breaking. For more than half of the breaking wave groups, after breaking, no obvious energy gain in the lower-frequency region immediately following breaking is observed. This result suggests that the energy gain in the lower-frequency region is possibly due to nonlinear energy transfer. Wave breaking may not necessarily increase the energy in the region, though it prevents the gained energy in this region from returning to other frequency regions. Spectral distribution of the energy variation after breaking is presented. The spectral change in the higher-frequency components, roughly $f/f_p = 1.2$–2.0, is due primarily to wave breaking and the dissipation in the range increases as wave breaking intensifies.

Complementary numerical tests are conducted, using a simple eddy viscosity model to simulate energy dissipation in breaking waves. The eddy viscosity model simulates well the surface elevations before and after wave breaking. It is also demonstrated that the predicted relative spectral change after breaking agrees well

with the experimental measurements, although the predicted wave frequency spectra at downstream locations have some discrepancies with the measurements. The possible cause of the disagreement may be applying to the free surface boundary conditions an effective viscosity that accounts for the total non-breaking energy dissipation, which is due to friction on the side tanks' walls and bottom, as well as the contact lines at the sidewalls in the experiments.

This work was supported by the US Office of Naval Research via grant no. N00014-05-1-0537. W.C. and Z.T. also gratefully acknowledge partial support from the Korea Science and Engineering Foundation via the WCU program (grant no. R31-2008-000-10045-0).

REFERENCES

BALDOCK, T. E., SWAN, C. & TAYLOR, P. H. 1996 A laboratory study of nonlinear surface waves on water. *Phil. Trans. R. Soc. Lond.* A **354**, 649–676.

BANNER, M. L. & PEIRSON, W. L. 2007 Wave breaking onset and strength for two-dimensional deep-water wave groups. *J. Fluid Mech.* **585**, 93–115.

BENJAMIN, T. B & FEIR, J. E. 1967 Disintegration of wave trains on deep water. Part 1. Theory. *J. Fluid Mech.* **27**, 417–430.

CHOI, W. 1995 Nonlinear evolution equations for two-dimensional surface waves in a fluid of finite depth. *J. Fluid Mech.* **295**, 381–394.

CHOI, W., KENT, C. P. & SCHILLINGER, C. 2005 Numerical modelling of nonlinear surface waves and its validation. *Adv. Engng Mech.* 94–110.

DRAZEN, D. A., MELVILLE, W. K. & LENAIN, L. 2008 Inertial scaling of dissipation in unsteady breaking waves. *J. Fluid Mech.* **611**, 307–332.

DUNCAN, J. H. 1981 An experimental investigation of breaking waves produced by a towed hydrofoil. *Proc. R. Soc. Lond. Ser.* A **377**, 331–348.

DUNCAN, J. H. 1983 The breaking and non-breaking wave resistance of a two-dimensional hydrofoil. *J. Fluid Mech.* **126**, 507–520.

GEMMRICH, J. R., BANNER, M. L. & GARRETT, C. 2008 Spectrally resolved energy dissipation rate and momentum flux of breaking waves. *J. Phys. Oceanogr.* **38**, 1296–1312.

JANSSEN, P. A. E. M. 2003 Nonlinear four-wave interaction and freak waves. *J. Phys. Oceanogr.* **33** (4), 863–884.

JIANG, L., PERLIN, M. & SCHULTZ, W. W. 2004 Contact-line dynamics and damping for oscillating free surface flows. *Phys. Fluids* **16** (3), 748–758.

KWAY, J. H. L., LOH, Y. S. & CHAN, E. S. 1998 Laboratory study of deep water breaking waves. *Ocean Engng* **25**, 657–676.

LAKE, B. M., YUEN, H. C., RUNGALDIER, H. & FERGUSON, W. E. 1977 Nonlinear deep-water waves: theory and experiment. Part 2. Evolution of a continuous wave train. *J. Fluid Mech.* **83**, 49–74.

LONGUET-HIGGINS, M. S. 1983 On the joint distribution of wave periods and amplitudes in a random wave field. *Proc. R. Soc. Lond.* A. **389**, 241–258.

MEI, C. C. 1983 *The Applied Dynamics of Ocean Surface Waves*. Wiley-Interscience.

MELVILLE, W. K. 1982 The instability and breaking of deep-water waves. *J. Fluid Mech.* **115**, 165–185.

MELVILLE, W. K. 1994 Energy-dissipation by breaking waves. *J. Phys. Oceanogr.* **24**, 2041–2049.

MELVILLE, W. K. 1996 The role of surface-wave breaking in air–sea interaction. *Annu. Rev. Fluid Mech.* **28**, 279–321.

MELVILLE, W. K., VERON, F. & WHITE, C. J. 2002 The velocity field under breaking waves: coherent structures and turbulence. *J. Fluid Mech.* **454**, 203–233.

MEZA, E., ZHANG, J. & SEYMOUR, R. J. 2000 Free-wave energy dissipation in experimental breaking waves. *J. Phys. Oceanogr.* **30**, 2404–2418.

NEPF, H. M., WU, C. H. & CHAN, E. S. 1998 A comparison of two- and three-dimensional wave breaking. *J. Phys. Oceanogr.* **28**, 1496–1510.

OCHI, M. K. 1998 *Ocean waves: The stochastic approach.*. Cambridge University Press.

ONORATO, M., CAVALERI, L., FOUQUES, S., GRAMSTAD, O., JANSSEN, P. A. E. M., MONBALIU, J., OSBORNE, A. R., PAKOZDI, C., SERIO, M., STANSBERG, C. T., TOFFOLI, A. & TRULSEN, K. 2009 Statistical properties of mechanically generated surface gravity waves: a laboratory experiment in a three-dimensional wave basin. *J. Fluid Mech.* **627**, 235–257.

PERLIN, M., HE, J. H. & BERNAL, L. P. 1996 An experimental study of deep water plunging breakers. *Phys. Fluids* **8** (9), 2365–2374.

PERLIN, M. & SCHULTZ, W. W. 2000 Capillary effects on surface waves. *Annu. Rev. Fluid Mech.* **32**, 241–274.

RAPP, R. J. & MELVILLE, W. K. 1990 Laboratory measurements of deep-water breaking waves. *Phil. Trans. R. Soc. Lond.* A. **331**, 735–800.

SHEMER, L., GOULITSKI, K. & KIT, E. 2007 Evolution of wide-spectrum unidirectional wave groups in a tank: an experimental and numerical study. *Eur. J. Mech. (*B/*Fluids*) **26**, 193–219.

SHEMER, L. & SERGEEVA, A. 2009 An experimental study of spatial evolution of statistical parameters in a unidirectional narrow-banded random wavefield. *J. Geophys. Res.* **114**, C01015.

SONG, J. B. & BANNER, M. L. 2002 On determining the onset and strength of breaking for deep water waves. Part I: Unforced irrotational wave groups. *J. Phys. Oceanogr.* **32**, 2541–2558.

TIAN, Z. G., PERLIN, M. & CHOI, W. 2008 Evaluation of a deep-water wave breaking criterion. *Phys. Fluids* **20**, 066604.

TIAN, Z. G., PERLIN, M. & CHOI, W. 2010 Energy dissipation in two-dimensional unsteady plunging breakers and an eddy viscosity model. *J. Fluid Mech.* **655**, 217–257.

TULIN, M. P. & WASEDA, T. 1999 Laboratory observations of wave group evolution, including breaking effects. *J. Fluid Mech.* **378**, 197–232.

WEST, B. J., BRUECKNER, K. A., JANDA, R. S., MILDER, D. M. & MILTON, R. L. 1987 A new numerical method for surface hydrodynamics. *J. Geophys. Res.* **92** (11), 803-11–824.

YAO, A. F. & WU, C. H. 2004 Energy dissipation of unsteady wave breaking on currents. *J. Phys. Oceanogr.* **34**, 2288–2304.

YOUNG, I. R. & BABANIN, A. V. 2006 Spectral distribution of energy dissipation of wind-generated waves due to dominant wave breaking. *J. Phys. Oceanogr.* **36**, 376–394.